applied sciences

MDPI

Article

The Measurement of the Impact Time to Evaluate the Plate Thickness

Giosuè Caliano *, Francesca Mariani, Michele Lo Giudice and Alessandro Salvini

Department of Civil, Computer Science and Aeronautical Technologies Engineering, Roma Tre University, 00146 Rome, Italy; francesca.mariani@uniroma3.it (F.M.); michele.logiudice@uniroma3.it (M.L.G.); alessandro.salvini@uniroma3.it (A.S.)

* Correspondence: giosue.caliano@uniroma3.it; Tel.: +39-0657337083

Abstract

The present study proposes a simple and low-cost indirect method for estimating the thickness of plates by measuring the contact time (T_C) generated by the impact of a free-falling sphere. The theoretical model has been developed on Tsai approximation of Zener's theory, which describes the dynamic interaction between the sphere and the plate taking in account the propagation of flexural waves. The methodology was validated through FEM simulations and through an extensive experimental campaign, where the contact times were measured using a simple electrical circuit. The results show excellent agreements between predicted and actual thicknesses, with relative errors below 3% for $\lambda < 1.5$ (where λ is the inelasticity parameter). For very thin plates and highly deformable materials, the above accuracy decreases due to flexibility and plastic deformation. We believe the proposed approach to be particularly promising in non-destructive testing applications within several scenarios, where speed, cost-effectiveness, and safety are essential requirements.

Keywords: collisions; contact time; impact; contact model; low-speed impact

1. Introduction

The study of impact processes, particularly the collision of spheres on plates, is a crucial area of scientific investigation, with significant relevance across various fields, including civil, mechanical, aerospace, and process engineering. These impacts play a vital role in diverse industries, such as chemicals, building, electrical, recycling, and energy. At a microscopic level, collisions are a permanent occurrence during macroscopic technical processes like handling, transportation, processing, and storage of particulate solids, directly influencing both product and process quality. Examples include particle-to-particle and particle-to-wall collisions in impact crushing, apparatus charging, fluidized or spouted beds, and pneumatic conveying [1]. Beyond industrial applications, these phenomena are observed in natural contexts, such as the aggregation of particles in protoplanetary disks, as well as in astronomy and space technology, for instance, impacts of spherical objects on spacecraft or collisions among space junk particles [2,3].

The term "impact" describes the process involving the collision of two or more objects. Typically, an impact is limited to collisions where the effect of both colliding bodies must be taken into account. The term "contact impact" is often used to emphasize the dynamic effects in contact phenomena. Contact impact problems are inherently nonlinear, since the actual contact surfaces are all unknown before the problem is solved. Consequently, the mathematical model of contact impact problems involves a system of nonlinear equations.

Academic Editor: Junhong Park

Received: 25 November 2025
Revised: 16 December 2025
Accepted: 19 December 2025
Published: 21 December 2025

Impact events are fundamentally characterized by changes in the state of motion, impulse, and energy of the colliding bodies, although momentum is conserved throughout. A key aspect of these collisions is energy dissipation, which can occur through several different mechanisms. Often, it is essential to consider the energy dissipated by elastic waves. During an impact, a pressure field develops at the contact area, generating stress waves that propagate inwards from the point of excitation. These elastic waves—including surface and body seismic waves—can transport energy, leading to a loss of kinetic energy from the system. When these waves encounter interfaces, they can be refracted or reflected, potentially returning to the contact area and causing additional energy dissipation. Understanding such energy dissipation mechanism is crucial, as it directly influences the impact behavior. This is often quantified by the so-called coefficient of restitution (CoR) which is recognized as a referred parameter for energy loss due to the motion in normal direction [4]. Several factors govern this behavior, including the material combination of the colliding bodies, their geometrical proportions (such as the ratio of sphere diameter to plate thickness), and the impact velocity. For instance, if enough kinetic energy is absorbed by the plate through elastic waves, the particle may adhere to the plate instead of rebounding [3].

Historically, various models have been developed to describe these complex interactions. The Hertzian impact theory [5] laid a foundational understanding for perfectly elastic collisions, but it generally assumes bodies of infinite dimensions and neglects energy dissipation by elastic wave propagation or viscous effects. In contrast, the Zener [6] model extended Hertz's theory by incorporating the effect of bending, considering energy dissipation primarily through flexural waves propagating radially from the contact area. This model is particularly relevant for impacts of spheres on large, thin plates where plate bending is significant. Further refinements, such as the Koller model [7], explore further into the details of elastic wave propagation (longitudinal and transversal waves) within plates, especially in the transitional regime between thin and massive plates, where the effects of multiple wave reflections have to be investigated. The Hunter model [8] also addresses energy dissipation due to elastic body and surface waves, transporting energy away from the impact point.

Through these studies, it has become evident that the ratio of sphere diameter to plate thickness and the specific material properties of both the sphere and the plate strongly influences the energy dissipation and the resulting coefficient of restitution. Conversely, the influence of the impact velocity on the coefficient of restitution can be made comparatively negligible under certain conditions.

Impact events can be classified based on the speed (low, high, ballistic, and hypersonic) at which they occur. Low-speed impact (<30 m/s) can describe situations such as a falling ball, while high-speed impact (30–250 m/s) can include a bird colliding with an airplane. Ballistic impact events include situations such as a bullet fired from a weapon at speeds greater than 250 m/s. Finally, orbital debris traveling through space at speeds up to 15 km/s is considered a hypervelocity impact event.

In the present paper only low-speed impact problems (<10 m/s) will be addressed. In particular, an indirect method for measuring the thickness of a plate subjected to an impact with a sphere falling freely from a certain height will be developed, by measuring the so-called "contact time". Such parameter, that indicates the duration of the contact between two solids, is influenced by several factors such as heat transfer, friction, and wear, and depends on the specific materials and interaction forces. Within simulations, contact laws describe the relationship between force and displacement over time during contact. A typical application is to measure the thickness of a tank or a screen from the outside of the surface (without need to access the inside) with a good degree of accuracy, without the use of sophisticated or expensive instrumentation, but only using a striker equipped

with an inexpensive accelerometer: essentially, it is a low-cost tester to measure thicknesses, usable even in hazardous environments subject to limitations. The only physical effect is sonic, based on the "noise" produced by the impact on the surface to be measured. This methodology has already produced similar low-cost and reliable instruments, developed by some of the authors of this paper, in the field of analysis and monitoring of frescoes in cultural heritage environment [9].

The technique developed in the present paper is based on a recent approximation of Zener's impact theory proposed by Tsai [10], which allows us to solve in a closed form the Zener nonlinear differential equation of motion. The approximate solution determines the relevant values of collision force, material displacement, velocity, and contact time. Ultimately, by applying an inverse method, it was possible to determine the thickness of the material subjected to impact based on the measured contact time. To this end, Section 2 develops the analytical theory on which the method is based, while Section 3 reports on an FEM model developed to verify the predictions of the mathematical model. Section 4 describes the measurement of the impact time and the related experimental setup, and finally, Section 5 analyzes the results and discusses possible improvements and limitations of the method described.

2. Theory of Impacts

Hunter [8] provided the expression for the contact force, $F_c(t)$, generated during the impact of a rigid spherical striker with radius b and mass m_1 against a flexible plane surface of a semi-infinite solid, as a function of the relative approach "α" between the striker and the impacted surface [6], in function of the time t:

$$F_c(t) = k\alpha(t)^{\frac{3}{2}} \tag{1}$$

where

$$k = \frac{4}{3}\sqrt{b}\left(\frac{(1-v_1^2)}{E_1} + \frac{(1-v^2)}{E}\right)^{-1} \tag{2}$$

ν_1, ν, and E_1, E are Poisson's ratios and elasticity moduli of the impacting sphere and the impacted object, respectively. The relative approach $\alpha(t)$ represents the measure of the penetration of the sphere during the impact (Figure 1).

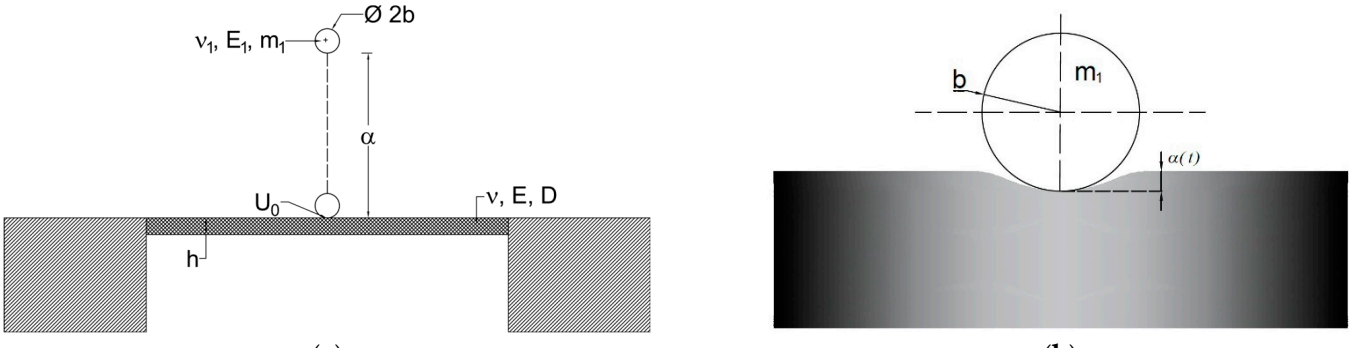

Figure 1. In (**a**), the conceptual scheme of the free fall impact of a spherical striker against a plane surface of thickness h; in (**b**) the rigid sphere impacting the thin flexible surface of the plate, with the indication of the relative approach "α" between the striker and the impacted surface.

When the sphere makes contact with the surface, $\alpha(0) = 0$, and then it increases with deformation. After the contact time Tc, $\alpha(t)$ returns to zero when the sphere detaches the surface. In particular, the trend of $\alpha(t)$ follows a typical curve of the elastic impact:

- Start of impact: at $t = 0$, we have $\alpha(0) = 0$;
- Compression phase: $\alpha(t)$ increases with surface deformation and the simultaneous generation of contact force Fc;
- Point of maximum compression: $\alpha(t)$ reaches a maximum value α_{max} when the relative velocity between the sphere and the surface goes to zero;
- Decompression phase: $\alpha(t)$ decreases as the sphere releases elastic energy and begins to rebound;
- End of impact: at $t = Tc$ we have $\alpha(Tc) = 0$, i.e., the sphere detaches from the surface.

The contact force expression presented in (1) is an extension of the well-known Hertz contact theory, originally developed for the static contact of curved bodies [3,11]. While (1) was derived for plates with semi-infinite thickness, it is also valid for thick plates or slabs, where the time required for elastic waves to reflect from the lower surface back to the impact area is significantly longer than the contact duration.

However, as the plate thickness or impedance decreases, the contact force between the sphere and the plate diverges significantly from the predictions of Hertz theory [5]. In the case of a sphere impacting a thin plate, the force–time history is determined by combining (1) with the plate's equation of motion [12–14]. Zener [6] derived the resulting nonlinear differential equation for a large plate, where reflections from the plate's boundaries return to the impact area only after the contact has ended. In order to introduce dimensionless variables, it is useful the transformations

$$\tau = \frac{t}{T}\,; \qquad \sigma = \frac{\alpha}{Tv_0} \tag{3}$$

where t is the time, T is a constant with dimensions of time: $T = \left(\frac{m_1}{kv_0^{\frac{1}{2}}}\right)^{\frac{2}{5}} = 0.311T_H$ and T_H is the duration of the impact predicted by Hertz theory for infinitely rigid surface and is given by $T_H = 2.9432\frac{\alpha_m}{v_0}$ where v_0 is the impact velocity and α_m is the maximum value of the relative displacement α, and is given by $\alpha_m = \left(\frac{5v_0^2 m_1}{4k}\right)^{\frac{2}{5}}$. Following Zener, the nondimensionalized solution of the (1) is given by:

$$\frac{d^2\sigma}{d\tau^2} + \left(1 + \lambda\frac{d}{d\tau}\right)\sigma^{\frac{3}{2}} = 0 \tag{4}$$

with the boundary conditions:

$$\left.\begin{array}{l} \sigma = 0 \\ \frac{d\sigma}{d\tau} = 1 \end{array}\right\}_{\tau=0}$$

Equation (4) depends on a dimensionless constant λ, called the "inelasticity parameter" (Equation (20) in [1]):

$$\lambda = \frac{\pi^{\frac{3}{5}}}{3^{\frac{1}{2}}}\left(\frac{r}{2h}\right)^2\left(\frac{v_0}{c'}\right)^{\frac{1}{5}}\left(\frac{\rho_1}{\rho}\right)^{\frac{3}{5}}\left(\frac{\frac{E_1}{(1-v_1^2)}}{\frac{E_1}{(1-v_1^2)} + \frac{E}{(1-v^2)}}\right)^{\frac{2}{5}} = \frac{3.218\cdot m_1}{T_H\cdot Z} \tag{5}$$

with c' the propagation velocity of quasi-longitudinal waves in thin plates, defined as in [1] by $c' = \sqrt{\frac{\frac{E}{(1-v^2)}}{\rho}}$, m_1 is the mass of the spherical striker, and Z is the acoustic impedance of the plate in the impacting position, given by [15]:

$$Z = 8\sqrt{D\rho h} \tag{6}$$

with D as the flexural rigidity, defined, as usual, by $D = \frac{Eh^3}{12(1-v^2)}$, ρ as the density and h the thickness of the plate.

The numerical solution of (4) is shown in Figure 2 (dashed curves) for some values of the inelasticity parameter (λ = 0, 0.25, 0.5, 1.0, 1.5). The approximate solution of (4) is derived by Tsai [10] for $0 \leq \lambda \leq 1.5$. In particular, the approximation with $n = 0.18$ was chosen, which minimizes the error between the approximated curves and the numerical solution of Equation (4) to approximately 7%.

$$\frac{F}{F_m} = \sigma^{\frac{3}{2}} = (1+n\lambda)^2 \left[\left(\lambda^{1.3} + 1 - \lambda \right) \frac{4\tau}{\tau_{el}} \left(1 - \frac{\tau}{\tau_{el}} \right) e^{-0.4\lambda\tau} \right]^{\frac{3}{2}} \tag{7}$$

where

$$\tau_{el} = 2.762 + 0.4568 e^{1.27\lambda} \tag{8}$$

is described by Muller [2]. Equation (7) is graphed in Figure 2 with continuous curves, for the same λ values used previously. Using (3) and (5), Equation (1) can be written as:

$$F = k(1+n\lambda)^2 \left[\left(\lambda^{1.3} + 1 - \lambda \right) \frac{4\tau}{\tau_{el}} \left(1 - \frac{\tau}{\tau_{el}} \right) e^{-0.4\lambda\tau} \right]^{\frac{3}{2}} (Tv_0)^{\frac{3}{2}} \tag{9}$$

and then,

$$F = \left(k^{\frac{2}{5}} m_1^{\frac{3}{5}} v_0^{\frac{6}{5}} \right)^{\frac{3}{2}} \cdot (1+n\lambda)^2 \left[\left(\lambda^{1.3} + 1 - \lambda \right) \frac{4\tau}{\tau_{el}} \left(1 - \frac{\tau}{\tau_{el}} \right) e^{-0.4\lambda\tau} \right]^{\frac{3}{2}} \tag{10}$$

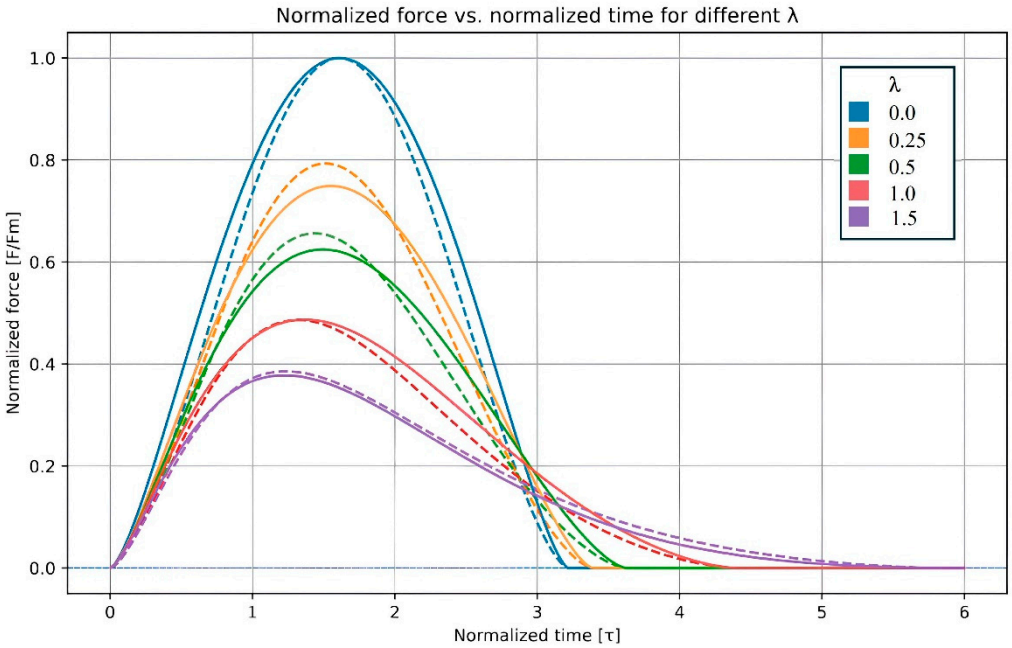

Figure 2. Comparison between the numerical solution of the differential Equation (4), dashed line, and the approximation described by Equation (7), solid line, as λ varies.

The force–time responses derived from (4) and (7) are shown in Figure 2 for different values of the inelasticity parameter λ. When λ is very small, the contact–time profile is similar to the square of a half-period sine wave [13]. As λ increases, the peak impact force is reduced, and the contact duration becomes longer during the latter half of the contact interval.

As can be seen in Figure 2, the approximation used models the trend of the curves well at least up to $\lambda = 1.5$. Our model starts with Equation (10), where we can note that the force–time history is equal to zero for $t = 0$ ($\tau = 0$) or when $t = T_C$. In this last case, $\tau = \frac{T_C}{T}$, and so Equation (10) becomes the following:

$$0 = \left(k^{\frac{2}{5}} m_1^{\frac{3}{5}} v_0^{\frac{6}{5}}\right)^{\frac{3}{2}} \cdot (1 + n\lambda)^2 \left[\left(\lambda^{1.3} + 1 - \lambda\right) \frac{4T_C}{T\tau_{el}} \left(1 - \frac{T_C}{T\tau_{el}}\right) e^{-\frac{0.4\lambda T_C}{T}}\right]^{\frac{3}{2}} \tag{11}$$

Then, Equation (11) is verified by $\left(1 - \frac{T_C}{T\tau_{el}}\right) = 0$, and if we use (8), we obtain:

$$\lambda = 0.7874 \cdot log\left[2.1891\left(\frac{T_C}{T} - 2.762\right)\right] \tag{12}$$

On the other hand, from (5), using the definition of T_H, and (6), we can write:

$$\lambda = \frac{3.218 \cdot m_1}{T_H Z} = \frac{3.218 \cdot m_1}{2.9432 \frac{\alpha_m}{v_0} \cdot 8\sqrt{D\rho h}} \tag{13}$$

and substituting D, and isolating h, we finally obtain:

$$h = 0.688 \cdot \sqrt{\frac{m_1 v_0 \sqrt{1 - \nu^2}}{\alpha_m \lambda \sqrt{E\rho}}} \tag{14}$$

Definitely, if we know T_C (contact time) and v_0 (impact velocity), m_1 (mass), b, ν_1, E_1 for the striker-sphere, and ν, E, and ρ for the plate, we can obtain the thickness h of the plate.

As can be seen from (14), $h \approx \sqrt{\frac{1}{\lambda}}$, i.e., the inelasticity parameter λ is inversely proportional to the second power of plate thickness. Moreover, for a fixed impact velocity, the impact–force amplitude grows nonlinearly with the plate thickness and the striker's mass, attaining the maximum value predicted by Hertz theory when the plate behaves as if it had semi-infinite thickness [15]. The maximum value of the normalized impact force decays exponentially with λ, as shown in Figure 2.

The equations used to calculate the thickness h of a plate, knowing the contact time T_C and the mechanical characteristics of the plate and the striker-sphere, are summed in (15).

As said before, we have estimated the error between the Tsai's approximated curves and the numerical solution of Equation (4) to approximately 7%.

$$\begin{cases} T = \left(\frac{m_1}{k v_0^{\frac{1}{2}}}\right)^{\frac{2}{5}} \\ k = \frac{4}{3}\sqrt{b}\left(\frac{(1-v_1^2)}{E_1} + \frac{(1-v^2)}{E}\right)^{-1} \\ \alpha_m = \left(\frac{5 v_0^2 m_1}{4k}\right)^{\frac{2}{5}} \\ \lambda = 0.7874 \cdot log\left[2.1891\left(\frac{T_C}{T} - 2.762\right)\right] \\ h = 0.688 \cdot \sqrt{\frac{m_1 v_0 \sqrt{1-\nu^2}}{\alpha_m \lambda \sqrt{E\rho}}} \end{cases} \tag{15}$$

We can use the given relations to a case reported in the literature, in particular the measure in Akay's experiment [15] (p. 642). We have a 1.905 cm diameter acrylic ball with an impact velocity of 0.62 m/s [15] (p. 646), impacting on a steel plate, and it is possible to estimate the contact time as T_C = 150 µs. Using some classical characteristics of the two

materials, as in Table 1, we calculate h = 1.56 mm, while in [15], it is 1.59 mm: consider that the material characteristics are not given in [15], so we relied on values found in the literature that may vary from experimental reality. There is excellent agreement between the calculated thickness and the experimental measurements reported in Akay's experiment. Moreover λ = 1.44, so Tsai's condition is also verified ($\lambda < 1.5$).

Table 1. Material's characteristics.

	Plate		
	ϱ [kg/m^3]	**E [GPa]**	**ν**
Akay's exp. [15]	7830	207.5	0.29
Steel plate	7500	205	0.3
Aluminum 1050/Al99.5	2700	69	0.33
Aluminum Type 2	2700	79	0.35
Brass CW508L/CZ108	8495	106	0.33
Brass Type 2	8400	100	0.33
Impact sphere (ball)			
Acrylic (Akay's exp. [15])	1190	3.3	0.37
Steel	7900	193	0.3

On the other hand, this condition is quite good for our application: in the case of λ = 1.5, the thickness is less than 1 mm, and so the measure is not possible to run, for obvious reasons of the fragility of the plate. If the elastic modulus of the plate is unknown, it is possible to determine it by the measure of the contact time T_C and knowing the force–time history.

If we indicate with A_1 the area under the (F,t) diagram, from the first impact instant and the maximum of the curve F, it is possible to demonstrate [16] that:

$$E = \frac{E^* E_1 \left(1 - v^2\right)}{E_1 + E^* \left(v_1^2 - 1\right)} \tag{16}$$

where b, E_1, m_1, v_1 are, respectively, the radius of curvature, the elastic modulus, the mass and the Poisson's ratio of the spherical mass, which strike the surface of the material to be analyzed; v was the Poisson's ratio of the analyzed material, and E^* is given by:

$$E^* = \sqrt{\left(\frac{2.87}{T_C}\right)^5 \frac{m_1^3}{b A_1}} \tag{17}$$

3. FEM Model

To investigate the impact dynamics and contact behavior, a finite element model (FEM) of the sphere-plate system was developed using a FEM software (Ansys 2025 R1). The model accounts for the material properties, geometry, and boundary conditions of both the impacting sphere and the steel plate, enabling the simulation of contact time and stress distribution during the impact event. In the context of the experiment, the contact time T_C represents the duration of the physical interaction between the sphere and the plate. During this interval, the plate undergoes a forced deformation that induces vibration. The direct estimation of the contact time T_C can be measured by plate displacement and deformation, while velocity and acceleration are obtained by differentiating the displacement response, but experimental tests can be affected by significant uncertainty, due to the very short duration of the phenomenon and the limitations of acquisition systems with adequate temporal resolution.

To validate the theoretical formulations of T_C, a finite element model of the pendulum–plate system was developed in a drop-test configuration. The numerical model focuses on the vibrational response of the plate subjected to an impact.

In the simulations, a steel sphere (mass 3.6 g) impacted plates made of steel (AISI-SAE 1008/1010, thickness 2.56 mm) and aluminum (Al 1050, 2.96 mm thickness and aluminum alloy, 3.0 mm thickness), released from a height of 150 mm (h_0) with a 90° release angle, including gravity. The mechanical properties of the materials are summarized in Table 1. An initial impact velocity of V_i = 1.71 mm/s was assigned to the sphere at the collision point. The contact pair was established between the sphere and its projection surface on the plate, as interface contact area. A contact friction coefficient (μ = 0.1) was applied on the normal direction [17]. A fixed support boundary condition (zero displacement and zero slope/rotation at the boundary) was applied to the plate perimeter. The finite element models were discretized using 3D solid elements. Particular attention was paid to mesh refinement in the impact zone, in order to ensure numerical stability of the time step and accurate representation of the rapidly evolving contact interaction, as shown in Figure 3.

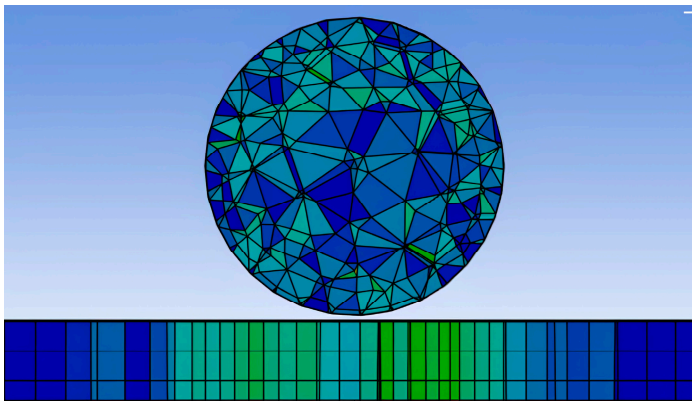

Figure 3. Finite element mesh of the sphere–plate system adopted in the Explicit Dynamics simulations. A local refinement was introduced in the impact region to capture the stress gradients and contact evolution.

For the steel plate model, the discretization consisted of approximately 23,000 nodes and 19,000 elements, with an average element size of 1.0 mm. Local refinement was applied at the plate–sphere interface to better capture stress gradients and velocity changes. The aluminum plate models required a finer mesh due to the higher compliance of the material and the plate geometries. In both cases, a combination of sweep and quad-dominant meshing was adopted, with local element sizes reduced to 0.5 mm in critical regions to ensure proper resolution of stress waves.

Across all models, mesh quality checks (aspect ratio, curvature capture, and element smoothing) were applied to maintain solution accuracy. The difference in mesh density among the cases reflects the balance between computational cost and the need to correctly represent the thin-plate geometry and the high-frequency content of the impact response.

The onset of contact can be identified by the instant when the plate velocity changes from zero to a nonzero value and the contact energy becomes significant. The results show that the directional velocity of the plate along the impact axis evolves from null values (pre-impact phase) to negative values (downward motion during contact), and then changes sign during rebound. The velocity sign reversal, as shown in Figure 4, is interpreted as the effective end of the contact interval. For the steel plate, the simulated T_C is in close agreement with theoretical predictions. For the aluminum plates, simulated T_C values are higher, consistent with the higher compliance of the material. The numerically obtained T_C aligns with the nonlinear models shown, while providing insight into the

complete kinematic and energetic evolution of the striker–plate interaction. FEM simulation therefore represents a valuable complementary tool to the theoretical framework presented in Section 2: by simulating the impact and extracting the contact time, it is possible to apply the analytical approach to infer plate thickness and elastic properties, even when direct physical measurement is not feasible.

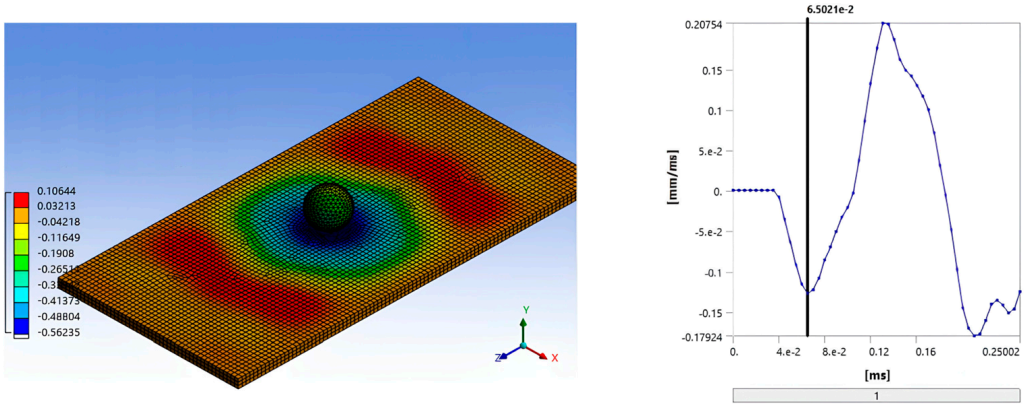

(**a**) (**b**)

Figure 4. Directional velocity of the plate along the impact axis obtained from FEM simulation. The contour plot (**a**) shows the deformation wave pattern at the moment of maximum interaction, while the velocity–time curve (**b**) highlights the contact interval. The velocity sign reversal at the first local minimum identifies the effective end of the contact duration between the sphere and the plate.

4. Impact Time Measurement

In order to develop a measure of impact time, the steel, brass, and aluminum plates (15 cm × 30 cm) were clamped at the edges using rectangular sandwich bolted together. The structure was designed to tension the inserted metal plates and thus create a sort of "drum". They were placed in a baffle, as shown in the schematic of the experimental apparatus in Figures 5 and 6.

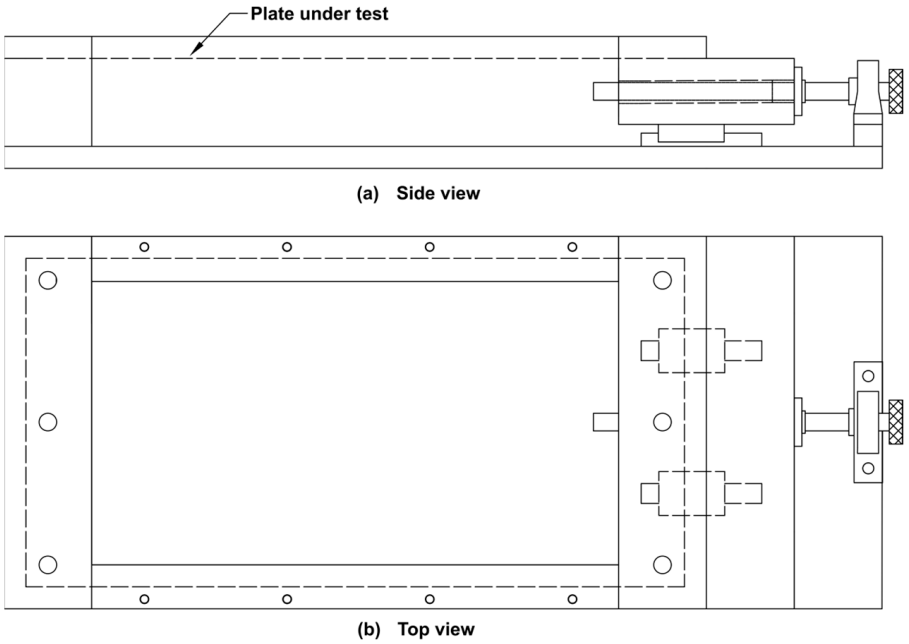

Figure 5. The structure designed (in (**a**) side and in (**b**) top view) to put in tension the metal plates under test.

Figure 6. The photos show the experimental setup used to measure the impact time.

The plates were impacted at their midpoints by a steel ball of 1.0 cm diameter. The steel sphere was hollow and had a threaded interior, allowing a thin, flexible electric conductor wire of negligible thickness to be connected to it. For this reason, the steel sphere was characterized separately, weighing it on a precision scale in such a way as to disregard the density-volume relationship, which in this case was not valid due to the presence of the internal threaded hole. For the investigation of the normal (low-velocity) impact behavior, the entire measuring structure, including the steel ball, was inserted into an electrical circuit of the type shown in Figure 7 in order to obtain an electrical "contact" signal on a scope between the ball impacting the plate and the plate itself, so as to measure the contact time with extreme precision. During each test, the sphere is dropped from a height h_0 such that it starts to fall freely without any initial velocity and rotation. The steel sphere is released using an electromagnet (em), controlled by a switch operated by the researcher, so as not to influence the fall of the sphere in any way by introducing rotations and initial moments.

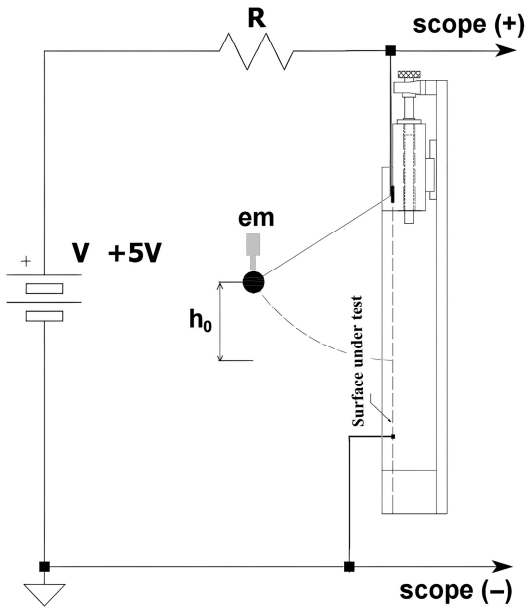

Figure 7. The schematic of the experiment to measure the impact time (electrically) between the striker-sphere and the plate using a scope.

After being released, the sphere undergoes free fall until it strikes the surface of the plate, which is positioned perpendicular to its trajectory. To measure the contact time, as previously mentioned, we used an oscilloscope to display the signal generated during the interval in which the sphere and plate are in contact: in effect, the sphere functions as a switch. To prevent any short-circuit between the negative and positive terminals, an ohmic resistor (R) was inserted into the switching circuit (see Figure 7). The contact time

measured experimentally corresponds to the interval during which the applied voltage is detected by the oscilloscope as the circuit remains closed (see Figure 8).

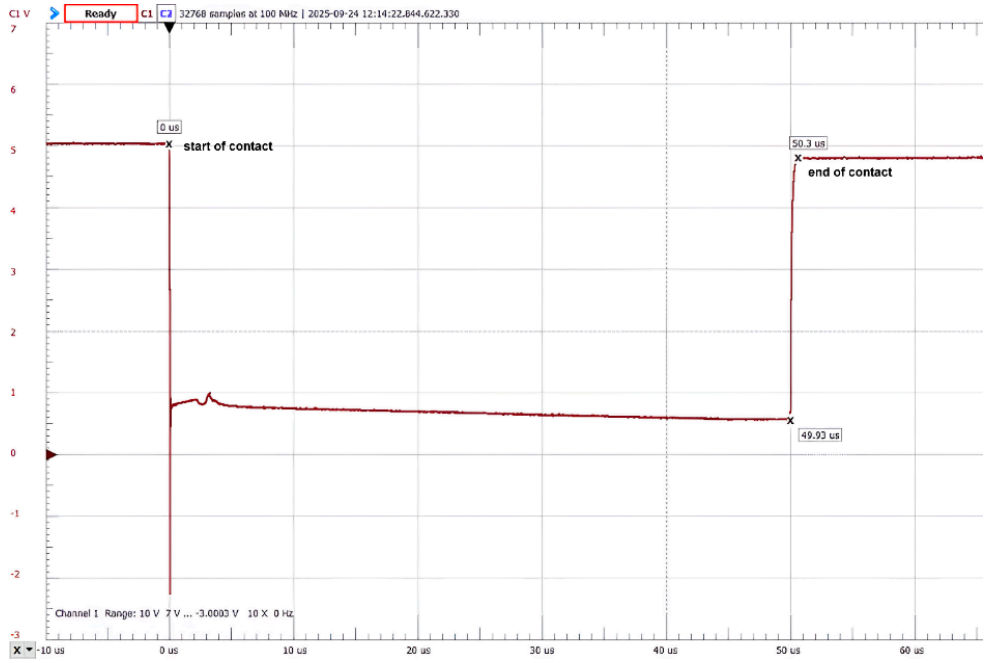

Figure 8. Oscilloscope recording of the signal during the impact event. The test was conducted on an Aluminum Type 2 plate, 3 mm thick, with a measured impact duration of 50.3 µs.

After the initial impact, the sphere rebounds to a maximum height, and then begins to fall again and produces a subsequent impact on the plate. This sequence continues through multiple impacts until the sphere either leaves the plate or comes to rest. To ensure accuracy and repeatability each measurement series was performed with more than 10 repeated impacts under identical conditions. The reported values of T_C and the corresponding reconstructed thickness represent the mean of these repetitions. The data dispersion was found to be small: for all tests within the model's validity range ($\lambda \leq 1.5$), the variability in the measured contact time T_C was limited, and the corresponding variation in the reconstructed thickness remained consistently low.

An Application of the Presented Method

The impact test is a vibration-based inspection method [18,19], in which a small hammer equipped with a force sensor delivers a controlled pulse on the surface. By measuring the impact force and consequently the impact time (T_C), variations in structural mobility due to localized damage can be detected. In addition to determinate the "health" of the material under examination, we want to measure its thickness at the measurement point. Indeed, in the past, tap testing (or coin tap testing [20,21]) was widely used in some industry sectors for assessing composite structures. This technique has progressed from a purely auditory procedure to an instrumented technique capable of producing quantitative maps of subsurface discontinuities—such as delaminations, debonds, and voids—in thin laminates, sandwich panels, and bonded joints, and also in composite materials, as stuccoes or frescoes. However, this technique only distinguishes between intact and damaged areas without providing information on their thickness, which is often of great importance in determining their state of conservation. On the other hand, machines that already implement this type of measurement (for example RD3 by WichiTech Industries [22], the Woodpecker by Mitsui Industries [23], the CATT designed at Iowa State University [24], and PICUS by the same authors [9]) can also measure the impact time

T_C, which is the parameter required to perform the measurement algorithm presented in paragraph 2, in addition to knowledge of the necessary mechanical parameters. These instruments operate by tapping the test surface with an impact hammer or tapper while measuring the corresponding contact time. This parameter can be obtained by integrating an accelerometer or force transducer within the tapping mass. Structural defects reduce local stiffness, resulting in a broader force–time pulse or, equivalently, a longer contact time. Consequently, intact rigid regions produce shorter readings, whereas damaged areas exhibit longer ones.

The force–time pulse captured by the accelerometer after each tap is converted into a voltage signal; the logic circuit then measures the half-amplitude width—i.e., the contact time—and displays it numerically [22]. Having developed in the past our measurement system called PICUS [9], the procedure described in the previous sections was simply added to the software stored in the machine in order to make the thickness measurement of the point under examination available. Obviously, as mentioned, the operator must also provide to furnish the mechanical quantities involved in the measurement, as described by Equation (15), in the appropriate menus of the software (Figure 9).

(a) **(b)** **(c)**

Figure 9. The PICUS tester for restorers with the modification introduced in the software for measuring surface thickness: in (**a**,**b**) a view of the instrument and screen when switched on, in (**c**) a typical measurement screen.

The system we developed aims to fill a technological gap in this domain while remaining practical for in situ use. Rather than replacing the operator's expertise, it is designed to complement it, providing objective confirmation—or reconsideration—of the tactile and auditory impressions obtained manually.

The results which, however, go beyond the authors' initial aims in this paper, obtained by introducing the mathematical algorithm based on (15) are good and will be presented in a future article, which will also discuss all the pros and cons of this type of measurement and, of course, the estimates of the errors that are inevitably present.

5. Results and Discussion

The experimental measurements and theoretical predictions of contact time were analyzed to evaluate the accuracy of the proposed indirect method for estimating plate thickness. Table 2 summarizes the experimental values of T_C, the actual plate thickness (h_{real}) measured with Mitsui thickness gauge, the estimated thickness using Equation (14) ($h_{estimated}$), the corresponding inelasticity parameter λ from Equation (12), and the percentage error between the real and estimated thickness.

Table 2. Measured Impact Time.

	Tc [μs]	h_{real} [mm]	$h_{estimed}$ by (14) [mm]	$\lambda_{estimed}$ by (12)	e %
Akay's exp. [15]	150	1.59	1.56	1.44	−1.88
Steel plate	35.2	2.56	2.58	0.61	+0.78
Aluminium 1050/Al99.5	55	2.96	2.90	1.05	−2.02
Aluminium Type 2	200.8	1.50	1.78	2.71	+18.6
Aluminium Type 2	49.96	3.00	3.02	0.94	+0.66
Brass CW508L/CZ108	216	1.08	1.26	2.85	+16.66
Brass Type 2	37.6	4.00	4.02	0.28	+0.5

The comparison between experimental and estimated values demonstrates the effectiveness of the method in a variety of plate materials and thicknesses. For most cases, the estimated thickness differs by less than 3% from the actual measured thickness, which is an excellent level of precision for a low-cost, non-invasive measurement technique. For instance, in the case of the steel plate, the actual thickness was 2.56 mm, while the estimated value was 2.58 mm, corresponding to a negligible error of +0.78%. Similarly, for aluminum Type 2 with a thickness of 3.00 mm, the method achieved an error of only +0.66%. These results confirm the strong correlation between the contact time and plate thickness, validating the theoretical framework based on the Tsai approximation of the Zener model. The best performance was observed for steel and aluminum plates with medium thickness ($h > 2$ mm and $\lambda < 1.5$). In these conditions, the assumptions of the theoretical model are fully satisfied, and the sphere-plate system behaves close to the ideal conditions assumed in the derivation. Conversely, higher errors were observed for very thin plates, such as brass CW508L/CZ108 and aluminum Type 2 with $h = 1.50$ mm and $h = 1.08$ mm, where the error reached +18.6% and +16.66%, respectively. These deviations are primarily due to the increased flexibility and fragility of thin plates, which amplify edge effects and boundary condition sensitivities. In these cases, the inelasticity parameter exceeded the limit of validity for the Tsai approximation ($\lambda < 1.5$), introducing non-linearities that were not fully captured by the model. Furthermore, localized plastic deformations may have occurred during the impact, violating the purely elastic assumption of the theoretical framework.

The inelasticity parameter λ plays a crucial role in interpreting the results. As shown in Table 2, cases with $\lambda < 1.5$ exhibited reliable and consistent estimations, while those with $\lambda > 1.5$ tended to deviate significantly. This confirms the theoretical prediction that the approximation is only valid within a specific range of λ. For example, in Akay's reference experiment, where $\lambda = 1.44$, the estimated thickness was 1.56 mm compared to the actual 1.59 mm, with a relative error of −1.88%. This excellent agreement validates both the mathematical approach and its practical application. However, for brass CW508L, where $\lambda = 2.85$, the model largely underestimated the complexity of the system, leading to a higher discrepancy.

The relationship $h \approx \sqrt{\frac{1}{\lambda}}$ highlights how small variations in λ strongly affect the estimated thickness for thin plates. Therefore, accurate measurement of contact time is critical to minimize propagated errors, especially in the transitional regime between thin and thick plates.

Tsai's approximation reproduces the numerical solution of Zener's nonlinear differential equation with a maximum discrepancy of approximately 7% in the normalized force–time history. However, this error does not directly represent the uncertainty introduced in the calculation of the inelasticity parameter λ, nor in the final estimation of the plate thickness h. The identification procedure adopted in this paper determines λ from the measured contact time T_C through Equation (12), which depends on the zero-crossing

of the contact-force waveform rather than its amplitude. Consequently, the inversion is inherently less sensitive to Tsai's 7% force approximation error.

To quantify this effect, a numerical sensitivity analysis was performed by evaluating the logarithmic derivative (see Appendix A)

$$r(\lambda) = \frac{\partial \ln(\sigma)}{\partial \ln(\lambda)} \tag{18}$$

where $r(\lambda)$ is the sensitivity coefficient, i.e., the ratio between the relative error of σ and the relative error of λ, computed at the peak of the nondimensional displacement response $\sigma(\tau)$. Propagating Tsai's 7% force error through the nonlinear chain

$$\frac{F}{F_m} = \sigma(\tau)^{\frac{3}{2}} \qquad \frac{\Delta\lambda}{\lambda} = \frac{2}{3r(\lambda)}\varepsilon_F \qquad h \propto \lambda^{-1/2} \tag{19}$$

yields the relative uncertainty

$$\left|\frac{\Delta h}{h}\right| = \frac{\varepsilon_F}{3|r(\lambda)|} \quad with\ \varepsilon_F = 0.07 \tag{20}$$

The resulting error curve (computed for $0.1 \leq \lambda \leq 1.5$ and using Tsai's approximation with $n = 0.18$ and Müller's expression for τ_{el}) shows a monotonic decrease in $|\Delta h/h|$ and increasing λ. Predicted thickness errors range from approximately 30% at $\lambda \approx 0.1$ to below 5% for $\lambda \gtrsim 1.2$. When compared to the experimental results of Table 2, the predicted range is consistent with observations: all specimens with $\lambda \leq 1.5$ exhibit thickness errors below 2%, demonstrating that the inversion based on contact time is significantly more robust than the 7% force error might initially suggest. Larger deviations occur only for $\lambda > 1.5$, where Tsai's approximation is no longer valid and the inversion becomes ill-conditioned.

A comparison between the theoretical error curve and the measured errors confirms that Tsai's approximation introduces negligible uncertainty in the thickness estimation for all cases lying within its validity domain. The full numerical analysis and the combined plot used for this comparison are shown in Figure 10.

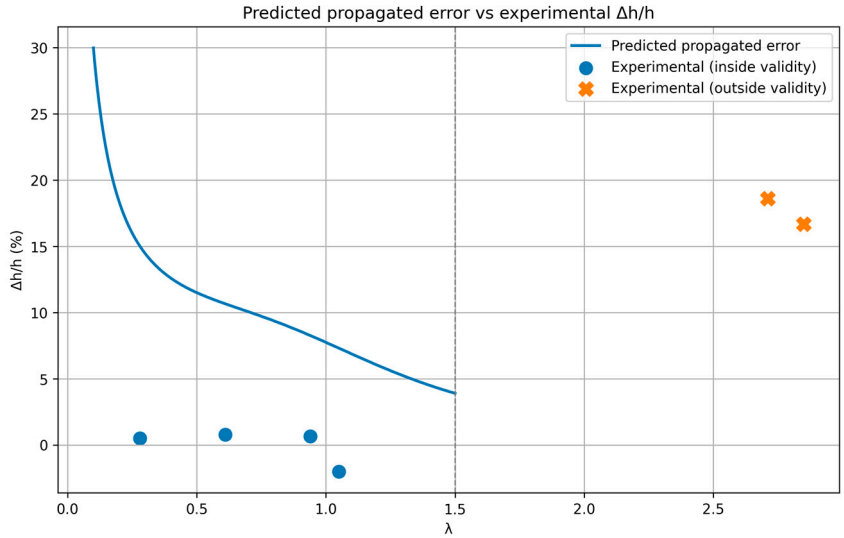

Figure 10. Comparison between the theoretical error curve and the errors measured inside and outside its domain of validity.

The finite element model (FEM) provided a complementary verification of the theoretical predictions. Simulated contact times were in close agreement with experimental data, particularly for steel and aluminum plates. For the steel plate, FEM simulations yielded a

T_C almost identical to the experimentally measured, confirming the validity of the theoretical assumptions for stiff materials. For more compliant materials, such as aluminum, the simulations predicted slightly higher contact times due to the greater flexural deformation of the plate. These differences highlight the influence of material compliance on the energy dissipation mechanisms and validate the need for a non-rigid plate model such as the Zener formulation. The FEM simulations provided further insights into the physical mechanisms governing the impact process. In particular, the simulations confirmed that the end of the contact interval corresponds to the reversal of the plate's velocity along the impact axis. Moreover, the propagation of flexural waves, clearly visible in the simulation results, supports the theoretical premise that energy dissipation through elastic wave generation plays a central role in extending the contact time relative to the Hertzian ideal case. The good agreement between FEM-predicted and experimentally measured T_C values reinforces the validity of the numerical model and demonstrates its potential as a complementary tool for refining the analytical approach.

However, the precision of the method depends on several factors. First, the boundary conditions may introduce variability in plate behavior due to clamping imperfections, especially for thin and flexible plates. In addition, the sphere release mechanism can introduce any initial rotation or lateral motion of the sphere, and so it could alter the impact dynamics and measured contact time. The material characterization by an accurate knowledge of the mechanical properties (E, ν, ρ) is essential for applying Equations (12) and (14). Uncertainty in these parameters directly affects the accuracy of thickness estimation. Higher values of λ amplify non-linearities associated with wave propagation and multiple reflections within the plate, which are not fully accounted for by the simplified analytical solution. Hence, when λ exceeds 1.5, the method's performance declines significantly.

In particular, the method assumes purely elastic behavior, which may not hold for thin plates or high-velocity impacts where plastic deformation occurs. For very small thicknesses ($h < 1.0$ mm), the fragility of the plate and the violation of the $\lambda < 1.5$ condition limit the applicability of the approach. The accuracy strongly depends on precise measurement of contact time and knowledge of material properties. These findings are consistent with previous studies on impact dynamics, which have highlighted the limitations of simplified models when dealing with highly compliant structures.

Finally, the proposed method was implemented in the PICUS measurement software, allowing reasonably good measurements to be obtained in agreement with other comparative measurements. In this paper, we do not show the measurements performed as they are the subject of a study that will be published later.

6. Conclusions

The results of this study confirm the feasibility of using contact time measurements to indirectly estimate the thickness of metallic plates impacted by a spherical striker. The experimental data, supported by theoretical modeling and FEM simulations, demonstrate that the method provides highly accurate estimations for a range of materials and geometrical configurations, particularly when the assumptions of the underlying model are satisfied. A key finding is the strong correlation between the inelasticity parameter λ and the reliability of thickness estimation. For cases where $\lambda < 1.5$, the approximation proposed by Tsai and implemented in this study accurately captures the sphere–plate interaction dynamics. In these conditions, the predicted thickness values are very close to the actual measurements, with errors generally below 3%. This level of agreement validates the theoretical framework based on the Zener model and confirms its suitability for practical applications such as non-destructive testing (NDT) of structural components.

From a practical perspective, the experimental setup developed in this study offers a simple and low-cost alternative to conventional thickness measurement techniques. Unlike high-speed imaging or laser-based systems, the electrical circuit used to measure contact time is straightforward to implement and provides microsecond resolution without complex instrumentation. This makes the approach particularly attractive for industrial applications where rapid and non-invasive assessment is required, such as monitoring the integrity of tanks, pipelines, or inaccessible structural elements. Furthermore, the introduction of a low-cost acceleration sensor axially to a spherical shutter that strikes the measurement surface can further simplify the structure of the low-cost measurement system, making it available not only for metal surfaces but also in cases where the surfaces are insulating or architectural. In fact, this study was carried out in response to the need to measure the thickness of detached surfaces in architectural coatings or ancient frescoes, a field in which the authors have extensive experience.

Overall, this study demonstrates that contact time is a reliable and sensitive parameter for characterizing sphere–plate interactions and for estimating plate thickness in a non-destructive manner. The combined use of analytical modeling, experimental validation, and numerical simulation provides a comprehensive understanding of the process and highlights both the strengths and limitations of the proposed method. Future work should focus on extending the model to incorporate viscoelastic or plastic effects, as well as exploring the influence of environmental variables such as temperature and surface roughness. Such developments would broaden the applicability of the technique and further enhance its utility for real-world engineering and diagnostic applications.

Author Contributions: Conceptualization, G.C.; Methodology, G.C. and F.M.; Investigation, G.C. and F.M.; Data curation, M.L.G.; Writing—original draft, G.C.; Writing—review and editing, G.C. and F.M.; Visualization, M.L.G.; Supervision, A.S.; review, A.S. All authors have read and agreed to the published version of the manuscript.

Funding: This research received no external funding.

Institutional Review Board Statement: Not applicable.

Informed Consent Statement: Not applicable.

Data Availability Statement: The original contributions presented in this study are included in the article. Further inquiries can be directed to the corresponding author.

Acknowledgments: The authors would like to thank Riccardo Borghi for his valuable help in reviewing the physical theory on which this paper is based and for his useful advice on improving the presentation; Gaia Caliano for reviewing the figures in the paper and collaborating on the creation of the experimental measuring device.

Conflicts of Interest: The authors declare no conflicts of interest.

Appendix A

Definition of the Sensitivity Coefficient

In the present work, the sensitivity of the nondimensional response $\sigma(\tau)$ to variations of the inelasticity parameter λ is expressed through the logarithmic derivative

$$r(\lambda) = \frac{\partial \ln(\sigma)}{\partial \ln(\lambda)}$$

This formulation is not arbitrary: it follows directly from the requirement that the error analysis must relate relative variations of σ to relative variations of λ. Indeed, for any differentiable function, the differentials $d(\ln\sigma) = d\sigma/\sigma$ and $d(\ln\lambda) = d\lambda/\lambda$ represent the

fractional (percent) variations of the two quantities. Their ratio therefore provides the local amplification factor between relative perturbations,

$$\frac{d\sigma/\sigma}{d\lambda/\lambda} = r(\lambda).$$

This identity is fundamental for inverse problems and uncertainty quantification, since it allows one to propagate a known relative error in the model response, $\Delta\sigma/\sigma$, into a corresponding relative error in the estimated parameter,

$$\frac{\Delta\lambda}{\lambda} = \frac{1}{r(\lambda)}\frac{\Delta\sigma}{\sigma}$$

Such a relation would not be obtained by using the ordinary derivative $\partial\sigma/\partial\lambda$, which measures absolute rather than relative variations and is therefore unsuitable for percent-based error propagation. The logarithmic sensitivity $r(\lambda)$ is thus the appropriate and standard measure for assessing the conditioning of the inversion from the response σ to the parameter λ, and it plays a central role in evaluating the robustness of the thickness estimation method.

With this in mind, we have calculated the expression of $r(\lambda)$ shown below for the reader's convenience.

$$r(\lambda,\tau) = \lambda\left[\frac{4}{3}\frac{n}{1+n\lambda} + \frac{1.3\,\lambda^{0.3}-1}{\lambda^{1.3}+1-\lambda} + \frac{\tau'_{el}(\lambda)}{\tau_{el}(\lambda)}\,\frac{-\tau_{el}(\lambda)+2\tau}{\tau_{el}(\lambda)-\tau} - 0.4\tau\right]$$

with $\boldsymbol{\tau'_{el}(\lambda)=0.580136\ e^{1.27\lambda}}$.

References

1. Müller, P.; Böttcher, R.; Russell, A.; Trüe, M.; Tomas, J. A novel approach to evaluate the elastic impact of spheres on thin plates. *Chem. Eng. Sci.* **2015**, *138*, 689–697. [CrossRef]
2. Müller, P.; Böttcher, R.; Russell, A.; Trüe, M.; Aman, S.; Tomas, J. Contact time at impact of spheres on large thin plates. *Adv. Powder Technol.* **2016**, *27*, 1233–1243. [CrossRef]
3. Boettcher, R.; Russell, A.; Mueller, P. Energy dissipation during impacts of spheres on plates: Investigation of developing elastic flexural waves. *Int. J. Solids Struct.* **2017**, *106–107*, 229–239. [CrossRef]
4. Haron, A.; Ismail, K.A. Coefficient of restitution of sports balls: A normal drop test. *IOP Conf. Ser. Mater. Sci. Eng.* **2015**, *36*, 012038. [CrossRef]
5. Hertz, H. Ueber die Berührung fester elastischer Körper. *J. Reine. Angew. Math.* **1882**, *92*, 156–171. [CrossRef]
6. Zener, C. Intrinsic inelasticity of large plates. *Phys. Rev.* **1941**, *59*, 669–673. [CrossRef]
7. Koller, M.G.; Kolsky, H. Waves produced by the elastic impact of spheres on thick plates. *Int. J. Solids Struct.* **1987**, *23*, 1387–1400. [CrossRef]
8. Hunter, S.C. Energy absorbed by elastic waves during impact. *J. Mech. Phys. Solids* **1957**, *5*, 162–171. [CrossRef]
9. Caliano, G.; Mariani, F.; Calicchia, P. Picus: A pocket-sized system for simple and fast non-destructive evaluation of the detachments in ancient artifacts. *Appl. Sci.* **2021**, *11*, 3382. [CrossRef]
10. Tsai, P.-K.; Li, C.-H.; Lai, C.-C.; Huang, K.-J.; Cheng, C.-W. Approximation Solution for the Zener Impact Theory. *Mathematics* **2021**, *9*, 2222. [CrossRef]
11. Love, A.E.H. *A Treatise on the Mathematical Theory of Elasticity*, 4th ed.; Dover: New York, NY, USA, 1944.
12. Goldsmith, W. *Impact (the Theory and Physical Behavior of Colliding Solids)*; Edward Arnold Publishers Ltd.: London, UK, 1960; pp. 82–144.
13. Karas, K. Platten unter seitlichem Stoss. *Ingenieur Archiv.* **1939**, *10*, 237–250. [CrossRef]
14. Goldsmith, W.; Lin, T.W.; Chulay, S. Plate impact and perforation by projectiles. *Exp. Mech.* **1965**, *5*, 385–404. [CrossRef]
15. Akay, A.; Latcha, M. Sound radiation from an impact-excited clamped circular plate in an infinite baffle. *J. Acoust. Soc. Am.* **1983**, *74*, 640–648. [CrossRef]
16. Grazzini, A. Sonic and Impact Test for Structural Assessment of Historical Masonry. *Appl. Sci.* **2019**, *9*, 5148. [CrossRef]
17. Wang, Y.; Peng, Q.; Song, H.; Wei, Y.G.; Liu, X. Semi-analytical model for elastoplastic impact of sphere on plate. *Int. J. Impact Eng.* **2025**, *198*, 105229. [CrossRef]

18. Sansalone, M.; Carino, N.J. Detecting delaminations in concrete slabs with and without overlays using the impact-echo model. *ACI Mater. J.* **1989**, *86*, 175–184.
19. Sansalone, M.; Streett, W.B. *Impact-Echo NDE of Concrete and Masonry*; Bullbrier Press: Ithaca, NY, USA, 2003.
20. Wu, H.D.; Siegel, M. Correlation of accelerometer and microphone data in the Coin Tap Test. In Proceedings of the Instrumentation and Measurement Technology Conference, Venice, Italy, 24–26 May 1999; Volume 2, pp. 814–819.
21. Cawley, P.; Adams, R.D. The mechanics of the coin-tap method of non-destructive testing. *J. Sound Vib.* **1988**, *122*, 299–316. [CrossRef]
22. Georgeson, G.E.; Lea, S.; Hansen, J. Electronic tap hammer for composite damage assessment. In *Nondestructive Evaluation of Aging Aircraft, Airports, and Aerospace Hardware*; SPIE: Bellingham, WA, USA, 1996; pp. 328–338.
23. Mitsuhashi, K.; Jyomuta, C.; Oka, F.; Nishikawa, H. Method and Apparatus for Impact-Type Inspection of Structures. U.S. Patent No. 5048320, 17 September 1991.
24. Hsu, D.K.; Barnard, D.J.; Peters, J.J.; Hudelson, N.A. Non-Destructive Inspections and the Display of Inspection Results. U.S. Patent No. 6327921B1, 11 December 2001.